Breakdown of long-range temporal dependence in default mode and attention networks during deep sleep

Enzo Tagliazucchi[a], Frederic von Wegner[a], Astrid Morzelewski[a], Verena Brodbeck[a], Kolja Jahnke[a], and Helmut Laufs[a,b,1]

[a]Department of Neurology and Brain Imaging Center, Goethe University, 60528 Frankfurt am Main, Germany; and [b]Department of Neurology, Schleswig Holstein University Hospital, 24105 Kiel, Germany

Edited by Marcus E. Raichle, Washington University in St. Louis, St. Louis, MO, and approved August 9, 2013 (received for review July 7, 2013)

The integration of segregated brain functional modules is a prerequisite for conscious awareness during wakeful rest. Here, we test the hypothesis that temporal integration, measured as long-term memory in the history of neural activity, is another important quality underlying conscious awareness. For this aim, we study the temporal memory of blood oxygen level-dependent signals across the human nonrapid eye movement sleep cycle. Results reveal that this property gradually decreases from wakefulness to deep nonrapid eye movement sleep and that such decreases affect areas identified with default mode and attention networks. Although blood oxygen level-dependent spontaneous fluctuations exhibit nontrivial spatial organization, even during deep sleep, they also display a decreased temporal complexity in specific brain regions. Conversely, this result suggests that long-range temporal dependence might be an attribute of the spontaneous conscious mentation performed during wakeful rest.

EEG–functional MRI | resting state | long-range correlations | multi-modal | consciousness

The human brain displays complex spatiotemporal patterns of energy-consuming activity, even in the absence of an explicit task or stimulation (1). Large efforts have been devoted to the study of spontaneous neural activity encoded in the slow (~0.1 Hz) fluctuations of the blood oxygen level-dependent (BOLD) signal, which are measured with functional MRI (fMRI). Nontrivial spatial organization of functional brain activity in resting state networks (RSNs) was consistently shown (2–4), comprising brain regions with high BOLD signal coherence and anatomical consistency with systems activated during task performance or stimulation (5).

Remarkably, although human nonrapid eye movement (NREM) sleep is characterized by impaired awareness and reduced conscious mentation, organization into RSNs is preserved in light sleep (6) and to a large extent, deeper sleep stages (7, 8) (*SI Appendix*, Fig. S8.1). In particular, the default mode network (DMN; a set of task-deactivated regions implied with internal conscious cognitive processes) (9, 10) was repeatedly observed during deep sleep, albeit with reduced frontal connectivity (11, 12). Although brain modules are preserved, even in the absence of conscious awareness, their functional integration is greatly impaired (8, 13, 14), which was predicted by an information integration account of consciousness (15). These results suggest that ongoing conscious mentation is not the only origin of RSN activity, whereas the level of consciousness is reflected in the interaction of functional networks.

However, brain activity is not completely characterized in the spatial domain only. fMRI BOLD signals display rich temporal organization, including scale-free 1/f power spectra and long-range temporal autocorrelations (16–18), with activity at any given time being influenced by the previous history of the system up to several minutes into the past. These landmarks of complex information processing and rapid adaptability are shared by many systems found in nature (19, 20). Evidence for such properties is also manifest in recordings from other modalities, such as EEG/magnetoencephalography (21, 22) and electrocorticography (23, 24). Long-range temporal correlations are ubiquitous in behavioral data (25–27), with behavioral long-range autocorrelations related to autocorrelations of underlying brain activity time courses (28).

The only studies to date addressing temporal properties of the BOLD signal during sleep have shown increased signal variance during early stages (29, 30); however, signal variance is, in principle, independent of long-range temporal correlation and thus, may fail to detect changes in temporal complexity. Given that long-range temporal memory is characteristic of the complex neural information processing taking place in the human cerebral cortex—and in particular, the spontaneous conscious mentation occurring during wakeful rest—we hypothesize that a breakdown of long-range temporal correlations will occur during the descent to deep sleep. In the present work, we put this hypothesis to test by studying, in a group of 63 subjects, changes in the voxelwise spatial distribution of the Hurst exponent (a measure of long-range temporal dependence) of fMRI BOLD signals across all stages of the human NREM sleep cycle, which are paralleled by decreased conscious awareness (31).

Results

Long-term dependence of BOLD signals was measured with the Hurst exponent (H), a single numerical quantity indicating the behavior of the autocorrelation function of a monofractal time series. [The behavior of a monofractal signal under a change of scale (*SI Appendix*, section 1) can be described by a single numerical exponent related to the fractal dimension. This behavior can be assumed as an adequate first approximation for fMRI time series (32).] For a stationary signal, $0 < H < 1$ holds with three qualitatively different cases: (i) $0.5 < H < 1$ (the signal displays long-range positive autocorrelation, with high values likely followed by high values and low values likely followed by low values), (ii) $0 < H < 0.5$ (the signal displays switching between consecutive time points, with high values likely followed by low values and vice versa), and (iii) $H = 0.5$ (the signal has exponentially decaying autocorrelation, including the possibility of no temporal correlation). A more detailed introduction to long-range temporal dependence and self-similarity can be found in *SI Appendix*, section 1. Simulating time series with a stochastic Gaussian process of known long-range temporal dependence (fractional Gaussian noise) (16), we first showed the suitability of detrended fluctuation analysis (DFA) (33) as a method to estimate H for time series of the same length as the BOLD signals used in our analyses (*SI Appendix*, Fig. S3.1) and showed that the estimation accuracy compares favorably with the

Author contributions: E.T. and H.L. designed research; E.T., F.v.W., A.M., V.B., K.J., and H.L. performed research; F.v.W., A.M., V.B., and K.J. contributed new reagents/analytic tools; E.T. and H.L. analyzed data; and E.T. and H.L. wrote the paper.

The authors declare no conflict of interest.

This article is a PNAS Direct Submission.

[1]To whom correspondence should be addressed. E-mail: h.laufs@neurologie.uni-kiel.de.

This article contains supporting information online at www.pnas.org/lookup/suppl/doi:10.1073/pnas.1312848110/-/DCSupplemental.

accuracy obtained for longer time series (*SI Appendix*, Fig. S3.2). (Because the BOLD signals under study comprise 5 min, it is important to verify that an accurate H estimate—compared with that estimate obtained from longer BOLD time series—is obtained.)

***H* Gradually Decreases from Wakefulness to Deep NREM Sleep.** We estimated H for all gray matter voxels and all stages of NREM sleep (wakefulness and N1, N2, and N3 sleep, with N1 being the earliest stage and N3 being the deepest stage). This analysis revealed a shift to exponentially decaying autocorrelation ($H = 0.5$) in the progression from wakefulness to deep sleep. In Fig. 1*A*, the H and σ^2 probability distributions for all epochs and voxels are shown as well as the average gray matter H and σ^2 values (in both cases, they are discriminated by sleep stage). The effect of sleep stage on H was highly significant ($F = 21.16$, $P < 10^{-9}$). Posthoc tests revealed significant differences between both wakefulness and all other sleep stages ($P < 10^{-3}$ in all cases). Significance for the comparison N1 vs. N3 sleep was$P = 0.0014$. Statistical significance was weaker for the difference between N2 and N3 sleep ($P = 0.0259$) and the difference between N1 and N2 sleep ($P = 0.116$). To compare the observed H values with the expected scanner-induced noise, we scanned a water phantom in the bore of the MRI scanner using the same sequence that was used for the sleep data acquisition. The H probability distribution for the water phantom sharply peaked around $H = 0.5$, indicating the lack of long-range temporal autocorrelations. Fig. 1*B* shows the averaged anatomical distributions of H and σ^2. H values in the range ≤ 0.5 are localized in the ventricles, whereas long-range temporal dependence was characteristic of the dynamics of cortical and subcortical gray matter. H and σ^2 exhibited a localized decrease and increase, respectively, which is discussed in the next section.

***H* During Deep Sleep Decreases in Frontoparietal DMNs and Attention Networks.** We performed a voxelwise comparison of H between wakefulness and all stages of NREM sleep. In Fig. 2*A*, we show the maps of statistical significance for the main effect of sleep stage for the mean of H together with results of posthoc tests between wakefulness and N2 and N3 sleep, and we assessed the directionality and sleep stage specificity of the effect. No voxels survived multiple comparison correction between wakefulness and light (N1) sleep. In contrast, a widespread decrease of H was observed for wakefulness vs. N2 and N3 sleep. Patterns of decreased H included parietal and frontal regions associated with DMNs and attention resting state networks. Additional decreases were located in the inferior temporal cortex and thalamus (regions sometimes included in the definition of the DMN) (2). During N3 sleep, the pattern was more widespread, including most of the occipital cortex and extending to larger regions in the parietal and frontal cortices. In *SI Appendix*, Table S9.1, information on local statistical significance maxima is presented. A replication of these results using a method in the time–frequency domain (wavelet analysis instead of DFA) is shown in *SI Appendix*, Fig. S10.1.

Variance During Deep Sleep Increases in Sensory Cortices. We analyzed differences in signal variance (σ^2), a measure linked to BOLD amplitude and therefore, spontaneous activation. Statistical significance maps of voxelwise comparisons between wakefulness and all sleep stages are shown in Fig. 2*B*. The effect of sleep stage in σ^2 was significant in the visual cortex. We found no difference (with respect to wakefulness) for N1 sleep; however, N2 sleep was marked by an increase in σ^2 that affected all sensory regions (visual, auditory, and somatosensory), and N3 sleep was characterized by an increase restricted to the visual cortex. In *SI Appendix*, Table S9.2, information on local statistical significance

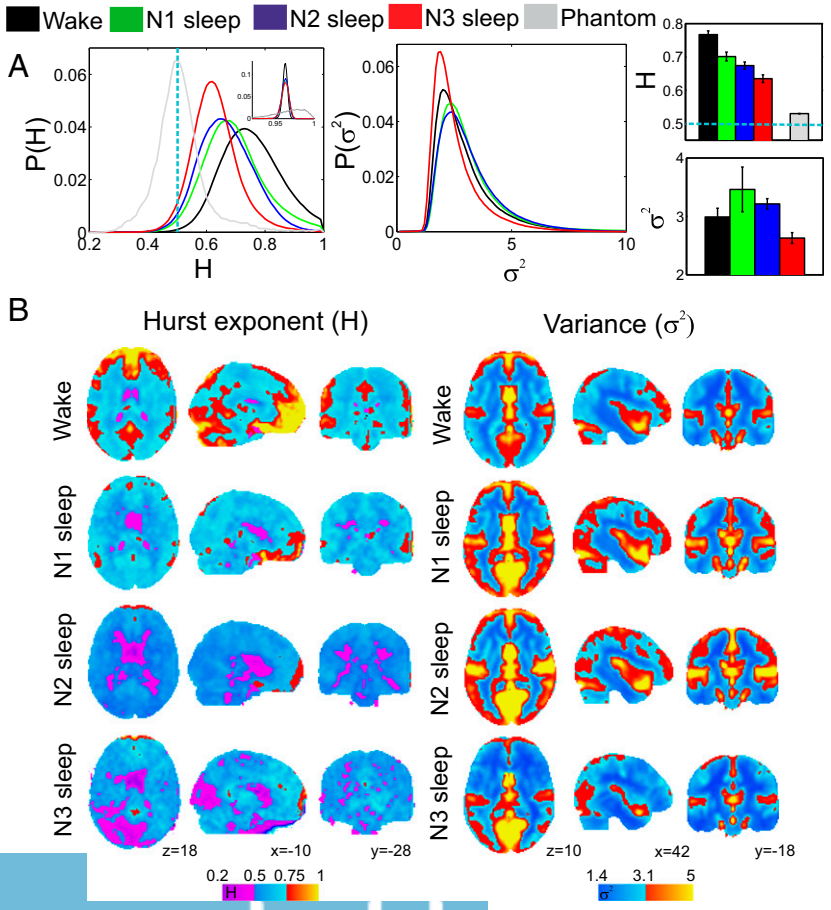

Fig. 1. BOLD signals gradually shift to short-range temporal correlations in the descent to deep sleep. (*A*, *Left*) Probability distributions for H (all gray matter voxels and all subjects) for all sleep stages and a water phantom. The probability distributions for the fluctuation function fitting error (R^2) are shown in *Inset*. (*A*, *Center*) Probability distributions for σ^2 by sleep stage (all gray matter voxels and subjects). (*A*, *Right*) Mean H (including phantom data for comparison) and σ^2 by sleep stage. Light blue dashed lines indicate $H = 0.5$, the value corresponding to exponentially decaying autocorrelation. (*B*) Spatial maps of average H and σ^2.

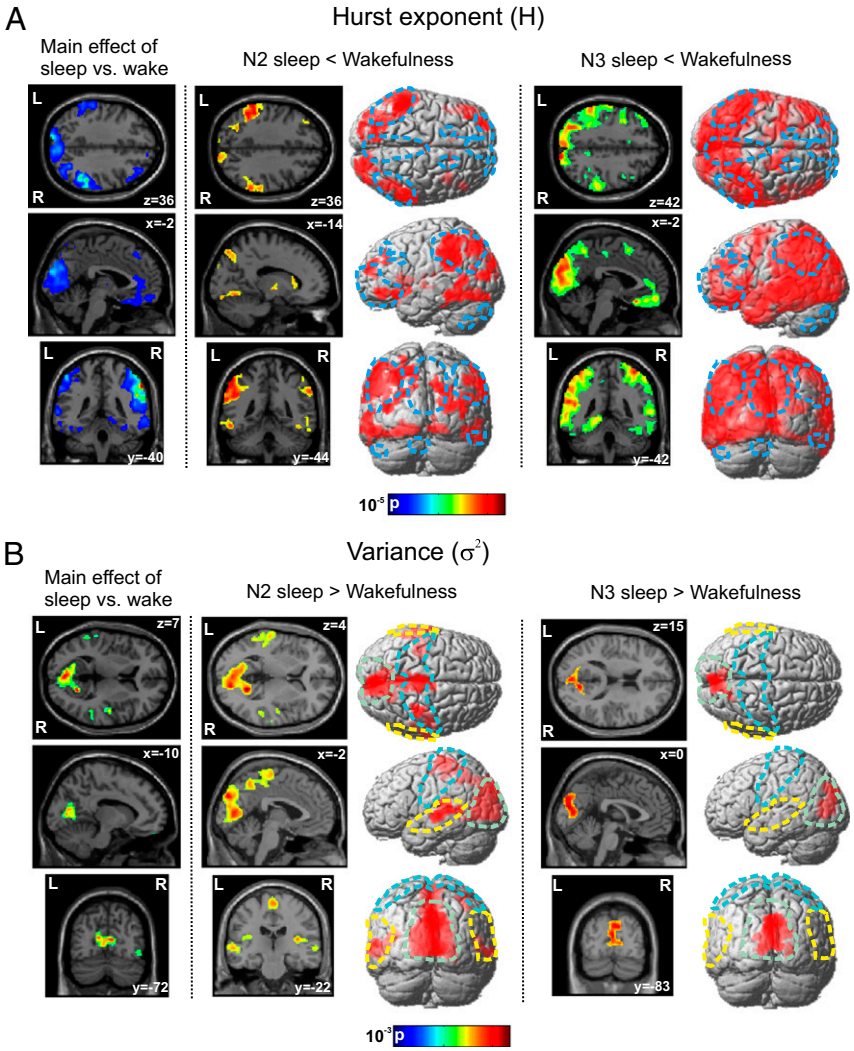

Fig. 2. Deep NREM sleep stages are characterized by specific spatial patterns of decreased H and increased variance. (*A*) Main effect of sleep stage on H and maps of statistically significant differences between wakefulness and N2 sleep and between wakefulness and N3 sleep. Results are presented overlaid onto an anatomical image and rendered on a 3D cortical surface. The blue dotted lines over the 3D rendering depict the DMN identified with ICA. Modified from ref. 3. Maps are thresholded at $P < 0.05$ [family wise error (FWE) cluster corrected]. (*B*) Main effect of sleep stage on σ^2 (signal variance) and maps of statistically significant differences between wakefulness and N2 sleep and between wakefulness and N3 sleep. Results are presented overlaid onto an anatomical image and rendered on a 3D cortical surface. The dotted lines over the 3D rendering depict the visual (light green), auditory (yellow), and sensory motor RSNs (light blue) found with ICA. Modified from ref. 3. Maps are thresholded at $P < 0.05$ (FWE cluster corrected).

maxima is provided. Because a straightforward estimation of σ^2 can be biased by H (*SI Appendix*, section 6), we provide a replication of these results using a method in the time–frequency domain (wavelet analysis, which robustly estimates σ^2), which can be found in *SI Appendix*, Fig. S10.2.

Different Spatial Patterns for Variance and *H* Differences. Visual inspection of Fig. 2 suggests that spatial patterns associated with H decrease and spatial patterns associated with σ^2 increase are largely uncorrelated (especially for N2 sleep). In Fig. 3*A*, such patterns are rendered together for comparison. In Fig. 3*B*, the principle RSNs are shown, which are revealed by independent component analysis (ICA) from wakefulness data (RSNs obtained from other sleep stages are shown in *SI Appendix*, Fig. S8.1), highlighting the fact that the H decrease is mostly related to task-negative and attention regions and the σ^2 increase is mostly related to sensory cortices. This observation is quantified in Fig. 3 by computing the overlap (spatial correlation) between the maps of statistically significant differences and the RSNs identified in the same data. This analysis confirms that H decreases during N2 sleep are mostly confined to DMNs and attention networks, with smaller overlaps with other RSNs (including visual areas). N3 sleep is characterized by a more widespread H decrease, including the aforementioned networks and additionally, encompassing the visual RSN. However, maps of σ^2 increase only overlap with visual and sensorimotor RSNs during N2 sleep and the visual RSN during N3 sleep.

***H* and Variance Covary with Changes in EEG Spectral Content.** Information integration theories (15) predict impaired consciousness in the presence of bistable cortical dynamics (34), which are associated with the slowing of EEG during deep sleep. This prediction prompted us to analyze the relationship between the Δ-band (1–4 Hz), H, and σ^2. In Fig. 4*A*, we show the spatial significance maps for the correlation between H and variance with δ-power (averaged from all channels). H correlates negatively in frontoparietal regions resembling DMNs and attentional networks, whereas BOLD variance shows a positive correlation in visual areas only. In Fig. 4*B*, we show scatter plots of H and σ^2 vs. δ for all wake and sleep epochs included in the study. BOLD signals used to estimate H and σ^2 were extracted from seeds defined in *SI Appendix*, Tables S9.1 and S9.2, respectively, and include DMNs and primary sensory motor regions; in these regions of interest, δ-power predicts increased H and decreased σ^2, respectively.

Discussion

In this work, we show compromised frontoparietal temporal autocorrelation in deep sleep, a brain state characterized by diminished conscious awareness. Our results establish that this property is gradually diminished from wakefulness to deep sleep. DMNs and attention networks are affected in the deeper sleep stages, comprising anatomical patterns markedly different to those of networks exhibiting increased signal variance.

Ever since the earliest days of scalp EEG, the presence of slow- and high-amplitude waves has been used as an objective marker of

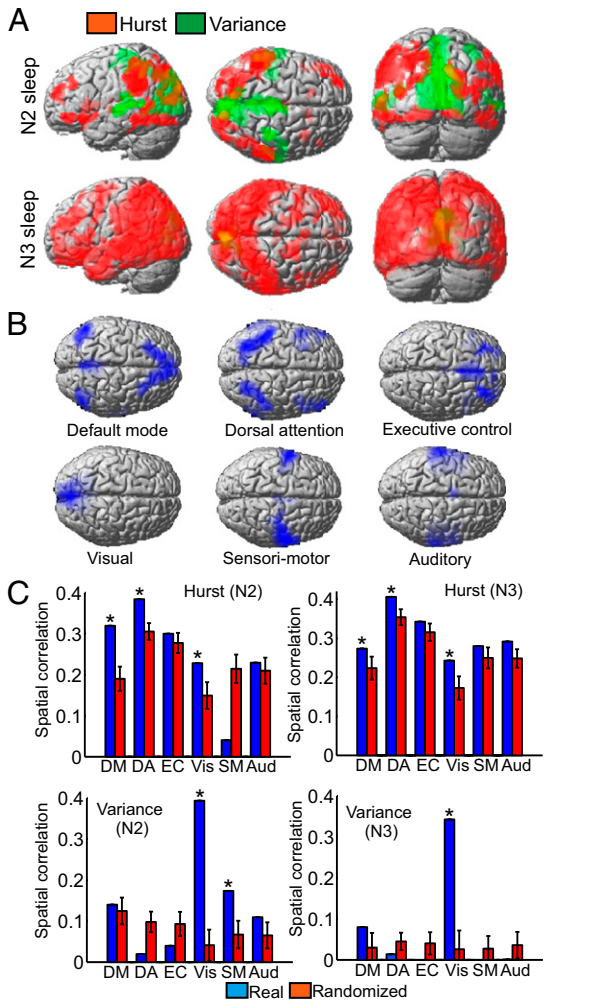

Fig. 3. Relationship between RSNs and patterns of change in temporal properties of the fMRI BOLD signal during deep sleep. (*A*) Maps of statistically significant differences in H and σ^2 (for N2 and N3 sleep vs. wakefulness) rendered together in a 3D cortical surface for comparison (overlapping regions are colored in yellow). (*B*) Rendering of maps representing six well-established RSNs (thresholded at $z = 2.3$): default mode, dorsal attention, executive control, visual, sensorimotor, and auditory. (*C*) Spatial correlation between maps of statistically significant differences in (*Left*) H and (*Right*) σ^2 and the RSNs revealed with ICA (for N2 and N3 sleep). Results were compared with 1,000 surrogate H and σ^2 maps with preserved first-order statistics (obtained by phase randomization), and an empirical P value was obtained by counting the instances of smaller correlation using the randomized versions (*$P < 0.05$, corrected), resulting in significant correlation of attention networks, DMNs, and visual RSNs with H significance maps during N2 and N3 sleep.

sleep depth (35). Long-range temporal memory is a landmark of power fluctuations in faster EEG and magnetoencephalography frequencies, such as α (8–12 Hz) or β (13–30 Hz) (21); in contrast, a decreased H exponent relative to the exponent of wakefulness is associated with the slow rhythms that herald the onset of deep sleep (36). Furthermore, sleep stage-dependent alterations in the 1/f electrocorticography power spectrum have recently been reported, which are closely linked to the autocorrelation regime (24).

Because the temporal resolution of fMRI is superseded by its high spatial specificity, it is a natural approach to focus on RSNs when studying how sleep-induced loss of conscious awareness impacts on resting state BOLD signal fluctuations. Although specific patterns of large-scale connectivity are characteristic of different NREM sleep stages (37) (in fact, allowing fMRI-based sleep staging) (38), ample evidence suggests that canonical RSNs are grossly preserved during sleep (7, 8) (*SI Appendix*, Fig. S8.1), possibly with weakened intranetwork connectivity in the case of the DMNs (11, 12). However, neural activity giving rise to the fMRI BOLD signal unfolds in the presence of a rich structural connectivity, which is known to be reflected in functional connectivity over relatively long temporal scales (39, 40). Therefore, patterns of anatomical connectivity could induce the homeostatic maintenance of BOLD coherence into RSN, even in the absence of complex temporal processing.

Recent work highlights the physiological relevance of long-range temporal dependence in the fMRI BOLD signal, showing anatomical specificity in the distribution of H exponents, correlation with brain glucose metabolism, and modulation by task performance (17, 18). Long-range temporal memory in the regional BOLD signal has been related to spontaneous information processing during the wakeful resting state, and activation caused by cognitive performance results in a loss of this property (17). The observed breakdown in the autocorrelation of BOLD fMRI during deep NREM sleep is unlikely related to increased BOLD activation; on the contrary, evidence exists that transient episodes of diminished conscious awareness imply deactivation of default mode areas (41, 42). BOLD variance, an index measuring intensity of activity fluctuations, is not affected by sleep in the frontoparietal network related to H changes. Task-induced deactivation also reduces long-range correlations (17), which could indicate an optimal dynamic range during wakeful rest. Taking this last observation into account, we speculate that long-range temporal memory is an essential characteristic of the unrestrained cognition occurring during the conscious, wakeful resting state, which can be suppressed by either loss of conscious awareness (as in deep NREM sleep) or focusing in demanding cognitive tasks.

The variance of spontaneous fMRI BOLD signal fluctuations also shows spatial specificity across the human cerebral cortex and decreases during activation/deactivation; furthermore, a positive correlation between variance and H exponent has been shown for specific brain regions during wakefulness (17, 43). In the present work, we found patterns of increased BOLD signal variance during deep NREM sleep that are compatible with previous results found by other researchers but obtained only for N1 or early sleep (29, 30). We have also shown that H exponent and signal variance changes affect different networks during the deeper sleep stages. A possible source for the observed variance changes is the polymodal BOLD deactivation (44) induced by environmental stimuli during sleep (possibly having a role in sleep protection) (45), which could be repeatedly triggered by scanner noise or internal stimuli and thus, contribute to an increased signal variance in the sensory cortices.

In a previous EEG–fMRI study, we linked spontaneous BOLD fluctuations in the DMN to EEG 17–23 Hz β-activity and spontaneous BOLD fluctuations in an attentional network to decreasing 8–12 Hz α-activity (46). The present results are consistent with these findings, given that these fast frequencies disappear along the descent to deep sleep. These frequencies can also be nested with slowly fluctuating scalp potentials (24, 27). In particular, a possible neurophysiological substrate for our results can be found in the slow cortical potential (SCP), a slow (<4 Hz) fluctuation predominantly generated by synaptic activity at apical dendrites in superficial cortical layers (47). Similar correlation patterns between the SCP and fMRI BOLD signal have been reported, which were also maintained in states of greatly diminished conscious awareness, such as slow wave sleep (48). A functional role for the SCP in the generation of conscious awareness was recently suggested (47). We analyzed the H exponent of EEG amplitude envelopes for different frequency bands and found differences only in the β_2 - (17–23 Hz) and α-bands (8–12 Hz); there were no changes in the slower-frequency bands (these results are in *SI Appendix*, section 16 and Figs. S16.1–S16.3). This result is consistent with frequency-specific EEG–fMRI correlations (46). It is likely, however, that even slower frequencies (accessible

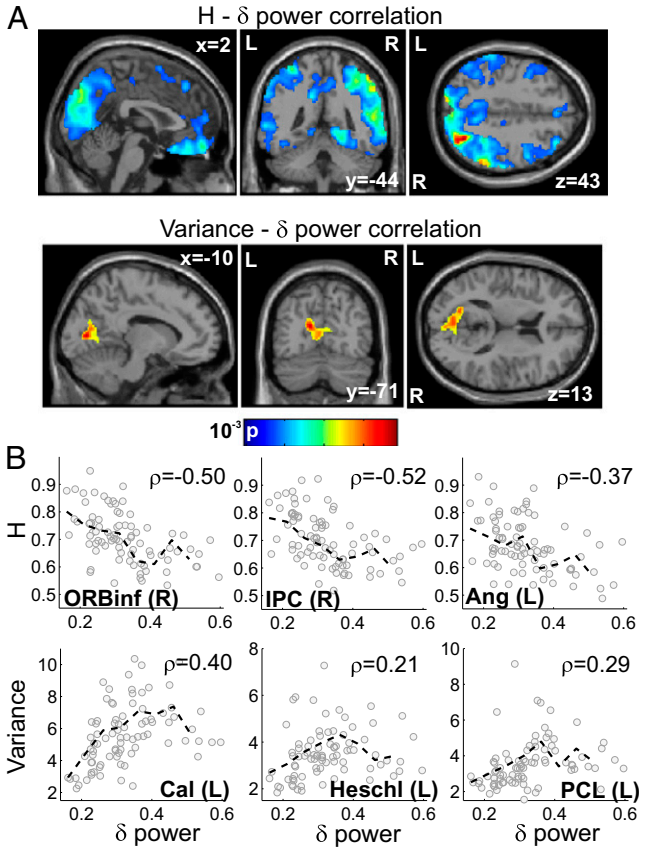

Fig. 4. EEG Δ-power (P_δ) predicts changes in BOLD fMRI temporal properties. (*A*) Statistical significance maps for the correlation between EEG δ-power (averaged across all channels) and *H* and BOLD variance. Maps are thresholded at $P < 0.05$ (FWE cluster corrected). (*B*) Scatter plots of *H* and BOLD variance vs. δ-power for three regions located in the DMN and three sensory regions (all selected from *SI Appendix*, Tables S9.1 and S9.2): right inferior frontal gyrus and orbital part (ORBinf; 44, 38, −6), right inferior parietal cortex (IPC; 52, −38, 56), left angular gyrus (ANG; −40, −60, −42), left calcarine sulcus (Cal; −2, −80, 12), left Heschl's gyrus (Heschl; −52, −10, 10), and left paracentral lobule (PCL; −2, −20, 68). Monotonous dependence was quantified with Spearman rank correlation [ρ; i.e., the linear correlation between ranked variables, which was in all cases significant ($P < 10^{-3}$)]; *x*, *y*, *z* indicate coordinates in Montreal Neurological Institute space.

through direct current measurements) have to be examined to establish changes in SCP autocorrelation during deep sleep.

Long-range temporal correlations and 1/f spectra are generic features predicted by self-organizing criticality, a theory of collective interactions that naturally accounts for many empirical observations about brain activity at different scales (20, 49). At the fMRI level, these features include the presence of long-range spatial correlations (50), power law-distributed avalanches of activity (51), and emergence of correlated structures resembling RSNs (52). The observed *H* exponent modulation by sleep prompts the possibility that self-organizing criticality in the human brain is not a trivial and unavoidable consequence of physical laws but rather, contributes to define the dynamical regime of conscious resting state activity, which can be changed during altered states of consciousness. A recent study reported changes in the power law distribution of neural avalanches measured with intracranial recordings during deep sleep, which is also consistent with this conjecture (53).

In conclusion, the loss of conscious awareness occurring during human NREM sleep is associated with hindered integration of brain activity not only across space but also in the temporal domain. The unified perceptual scene that we experience at any given moment during consciousness is accompanied by a sense of temporal continuity. Our results suggest that long-term memory in the history of neural processing of specific brain regions is a temporal signature of the spontaneous conscious mentation performed during wakeful rest. The extension of our analyses to other states of impaired consciousness might improve the understanding of conscious awareness and its relationship with long-range temporal dependence, a topic deserving additional exploration.

Materials and Methods

EEG–fMRI Acquisition and Artifact Correction. EEG through a cap (modified BrainCapMR; Easycap) was recorded during fMRI acquisition (1,505 volumes of T2*-weighted echo planar images, repetition time/echo time = 2,080 ms/30 ms, matrix = 64 × 64, voxel size = 3 × 3 × 2 mm^3, distance factor = 50%; field of view = 192 mm^2) at 3 T (Siemens Trio) with an optimized polysomnographic setting [chin and tibial electromyography, electrocardiogram, and electrooculography recorded bipolarly (sampling rate = 5 kHz, low pass filter = 1 kHz), 30 EEG channels recorded with FCz as the reference (sampling rate = 5 kHz, low pass filter = 250 Hz, high pass filter = 0.016 Hz), and pulse oxymetry; respiration recorded through sensors from the Trio (sampling rate = 50 Hz)] and MR scanner compatible devices (BrainAmp MR+, BrainAmp ExG; Brain Products). MRI and pulse artifact correction were performed based on the average artifact subtraction method (54) as implemented in Vision Analyzer2 (Brain Products) followed by objective (CBC parameters; Vision Analyzer) ICA-based rejection of residual artifact-laden components after average artifact subtraction resulting in EEG with a sampling rate of 250 Hz. Good quality EEG was obtained, which allowed sleep staging by an expert according to the American Academy of Sleep Medicine (AASM) criteria (55).

Subjects. A total of 63 nonsleep-deprived subjects was scanned in the evening (starting from ~8:00 PM) and preliminarily included in the study (written informed consent; approval by the local ethics committee). Eight subjects had no epochs of sleep and formed a dataset to test DFA on long (1,500 volumes) BOLD signals without vigilance switches; 55 subjects reached at least sleep stage N1. For these subjects, we scanned the hypnograms searching for epochs of contiguous sleep stages lasting longer than 5 min (150 volumes). Subjects having only epochs of wakefulness fulfilling this criterion were excluded from the analyses, leading to a more balanced dataset of 39 subjects; 70 epochs of wakefulness, 42 epochs of N1 sleep, 47 epochs of N2 sleep, and 38 epochs of N3 sleep were included in the analyses. The detailed sleep architecture of each participant can be found in *SI Appendix*, Table S7.1.

Data Preprocessing. Using Statistical Parametric Mapping 8, Echo Planar Imaging (EPI) data were realigned, normalized (Montreal Neurological Institute space), and spatially smoothed (Gaussian kernel, 8 mm^3 full width at half maximum). Cardiac-, respiratory-, and motion-induced noises were regressed out using the RETROICOR method (56). Short periods (up to 6 volumes) of large (>0.25 mm translational motion with respect to a reference volume) motion events were eliminated from the analysis using the information in ref. 57. Data were band pass-filtered in the range of 0.01–0.10 Hz using a sixth-order Butterworth filter. An ICA was performed on the dataset comprising all epochs from each sleep stage using MELODIC FSL. Components reproducing six well-established RSNs (3) were thresholded at Z = 2.3.

***H* Exponent Estimation with DFA.** DFA (33) quantifies the presence of long-range temporal dependence in a time series, and it has been developed to account for possible nonstationarities (local trends) in the data (a general discussion on long-range temporal dependence is in *SI Appendix*, section 1). Given x_i, a series of consecutive measurements, the first step is to subtract the mean and obtain the cumulative sum of the signal:

$$X_t = \sum_{i=1}^{t} (x_i - \langle x \rangle), \quad [1]$$

where $\langle , \rangle$ denotes time average. Next, this signal is divided into non-overlapping time windows of length *L*, and each is labeled Y_j^k, where *j* indexes measurement number (ranging from 1 to *L*) and *k* indexes the time window (ranging from 1 to the length of X_t divided by *L*). Then, a linear function is fitted using least squares in each time window Y_j^k, yielding the slope (a^k) and intercept (b^k) parameters. The signal is detrended by subtracting the best linear fit, and then, the rmsd of this signal (i.e., the fluctuation from the trend) is computed as follows:

$$F^k = \sqrt{\frac{1}{L}\sum_{j=1}^{L}\left(Y_j^k - a^k j - b^k\right)^2}. \quad [2]$$

The F^k values are then averaged across all time windows to yield the fluctuation function, $F(L)$. For a scale-free or self-affine signal, $F(L) \propto L^{\alpha}$. In the case of $0 < \alpha < 1$, the time series is stationary, and we identify α with H. We have applied DFA with window sizes of 15, 25, 30, 50, and 75, which were selected using the procedure described in *SI Appendix*, section 2. The procedures followed to assess the goodness of fit are also described in *SI Appendix*, section 2.

Statistical Testing. To guarantee statistical independence, H exponent and variance maps of every subject were averaged across epochs, yielding $n = 27$ (wakefulness), $n = 20$ (N1 sleep), $n = 24$ (N2 sleep), and $n = 13$ (N3 sleep). The effect of sleep stage on H and σ^2 was assessed using ANOVA tests. To assess the directionality of the effect, posthoc Student t tests were performed. Corrections for voxelwise multiple comparisons using random Gaussian field theory were performed with Statistical Parametric Mapping 8.

ACKNOWLEDGMENTS. We thank Torben E. Lund for providing an MATLAB implementation of the RETROICOR method; Sandra Anti, Ralf Deichmann, and Steffen Volz for extensive MRI support; anonymous reviewers for many helpful comments; and all subjects for their participation. This work was funded by Bundesministerium für Bildung und Forschung Grant 01 EV 0703 and the Landes-Offensive zur Entwicklung Wissenschaftlich-ökonomischer Exzellenz (LOEWE) Neuronale Koordination Forschungsschwerpunkt Frankfurt (NeFF).

1. Raichle ME (2006) Neuroscience. The brain's dark energy. *Science* 314(5803):1249–1250.
2. Greicius MD, Krasnow B, Reiss AL, Menon V (2003) Functional connectivity in the resting brain: A network analysis of the default mode hypothesis. *Proc Natl Acad Sci USA* 100(1):253–258.
3. Beckmann CF, DeLuca M, Devlin JT, Smith SM (2005) Investigations into resting-state connectivity using independent component analysis. *Philos Trans R Soc Lond B Biol Sci* 360(1457):1001–1013.
4. Damoiseaux JS, et al. (2006) Consistent resting-state networks across healthy subjects. *Proc Natl Acad Sci USA* 103(37):13848–13853.
5. Smith SM, et al. (2009) Correspondence of the brain's functional architecture during activation and rest. *Proc Natl Acad Sci USA* 106(31):13040–13045.
6. Larson-Prior LJ, et al. (2009) Cortical network functional connectivity in the descent to sleep. *Proc Natl Acad Sci USA* 106(11):4489–4494.
7. Boly M, et al. (2008) Intrinsic brain activity in altered states of consciousness: How conscious is the default mode of brain function? *Ann N Y Acad Sci* 1129:119–129.
8. Boly M, et al. (2012) Hierarchical clustering of brain activity during human nonrapid eye movement sleep. *Proc Natl Acad Sci USA* 109(15):5856–5861.
9. Raichle ME, et al. (2001) A default mode of brain function. *Proc Natl Acad Sci USA* 98(2):676–682.
10. Spreng RN, Grady CL (2010) Patterns of brain activity supporting autobiographical memory, prospection, and theory of mind, and their relationship to the default mode network. *J Cogn Neurosci* 22(6):1112–1123.
11. Horovitz SG, et al. (2009) Decoupling of the brain's default mode network during deep sleep. *Proc Natl Acad Sci USA* 106(27):11376–11381.
12. Sämann PG, et al. (2011) Development of the brain's default mode network from wakefulness to slow wave sleep. *Cereb Cortex* 21(9):2082–2093.
13. Spoormaker VI, Gleiser PM, Czisch M (2012) Frontoparietal connectivity and hierarchical structure of the brain's functional network during sleep. *Front Neurol* 3:80.
14. Tagliazucchi E, et al. (2013) Large-scale brain functional modularity is reflected in slow electroencephalographic rhythms across the human non-rapid eye movement sleep cycle. *Neuroimage* 70:327–339.
15. Tononi G (2008) Consciousness as integrated information: A provisional manifesto. *Biol Bull* 215(3):216–242.
16. Maxim V, et al. (2005) Fractional Gaussian noise, functional MRI and Alzheimer's disease. *Neuroimage* 25(1):141–158.
17. He BJ (2011) Scale-free properties of the functional magnetic resonance imaging signal during rest and task. *J Neurosci* 31(39):13786–13795.
18. Ciuciu P, Varoquaux G, Abry P, Sadaghiani S, Kleinschmidt A (2012) Scale-free and multifractal time dynamics of fMRI signals during rest and task. *Front Physiol* 3:186.
19. Bullmore E, et al. (2009) Generic aspects of complexity in brain imaging data and other biological systems. *Neuroimage* 47(3):1125–1134.
20. Chialvo DR (2010) Emergent complex neural dynamics. *Nature Phys* 6:744–750.
21. Linkenkaer-Hansen K, Nikouline VV, Palva JM, Ilmoniemi RJ (2001) Long-range temporal correlations and scaling behavior in human brain oscillations. *J Neurosci* 21(4):1370–1377.
22. Van de Ville D, Britz J, Michel CM (2010) EEG microstate sequences in healthy humans at rest reveal scale-free dynamics. *Proc Natl Acad Sci USA* 107(42):18179–18184.
23. Miller KJ, Sorensen LB, Ojemann JG, den Nijs M (2009) Power-law scaling in the brain surface electric potential. *PLoS Comput Biol* 5(12):e1000609.
24. He BJ, Zempel JM, Snyder AZ, Raichle ME (2010) The temporal structures and functional significance of scale-free brain activity. *Neuron* 66(3):353–369.
25. Gilden DL, Thornton T, Mallon MW (1995) 1/f noise in human cognition. *Science* 267(5205):1837–1839.
26. Shelhamer M, Joiner WM (2003) Saccades exhibit abrupt transition between reactive and predictive; predictive saccade sequences have long-term correlations. *J Neurophysiol* 90(4):2763–2769.
27. Monto S, Palva S, Voipio J, Palva JM (2008) Very slow EEG fluctuations predict the dynamics of stimulus detection and oscillation amplitudes in humans. *J Neurosci* 28(33):8268–8272.
28. Palva JM, et al. (2013) Neuronal long-range temporal correlations and avalanche dynamics are correlated with behavioral scaling laws. *Proc Natl Acad Sci USA* 110(9):3585–3590.
29. Fukunaga M, et al. (2006) Large-amplitude, spatially correlated fluctuations in BOLD fMRI signals during extended rest and early sleep stages. *Magn Reson Imaging* 24(8):979–992.
30. Horovitz SG, et al. (2008) Low frequency BOLD fluctuations during resting wakefulness and light sleep: A simultaneous EEG-fMRI study. *Hum Brain Mapp* 29(6):671–682.
31. Laureys S, Tononi G, eds (2011) *The Neurology of Consciousness: Cognitive Neuroscience and Neuropathology* (Academic, London).
32. Wink AM, Bullmore E, Barnes A, Bernard F, Suckling J (2008) Monofractal and multifractal dynamics of low frequency endogenous brain oscillations in functional MRI. *Hum Brain Mapp* 29(7):791–801.
33. Peng CK, Havlin S, Stanley HE, Goldberger AL (1995) Quantification of scaling exponents and crossover phenomena in nonstationary heartbeat time series. *Chaos* 5(1):82–87.
34. Balduzzi D, Tononi G (2008) Integrated information in discrete dynamical systems: Motivation and theoretical framework. *PLoS Comput Biol* 4(6):e1000091.
35. Loomis AL, Harvey EN, Hobart G (1935) Further observations on the potential rhythms of the cerebral cortex during sleep. *Science* 82(2122):198–200.
36. Acharya U R, Faust O, Kannathal N, Chua T, Laxminarayan S (2005) Non-linear analysis of EEG signals at various sleep stages. *Comput Methods Programs Biomed* 80(1):37–45.
37. Spoormaker VI, Czisch M, Maquet P, Jäncke L (2011) Large-scale functional brain networks in human non-rapid eye movement sleep: Insights from combined electroencephalographic/functional magnetic resonance imaging studies. *Philos Trans A Math Phys Eng Sci* 369(1952):3708–3729.
38. Tagliazucchi E, et al. (2012) Automatic sleep staging using fMRI functional connectivity data. *Neuroimage* 63(1):63–72.
39. Honey CJ, et al. (2009) Predicting human resting-state functional connectivity from structural connectivity. *Proc Natl Acad Sci USA* 106(6):2035–2040.
40. Greicius MD, Supekar K, Menon V, Dougherty RF (2009) Resting-state functional connectivity reflects structural connectivity in the default mode network. *Cereb Cortex* 19(1):72–78.
41. Laufs H, Lengler U, Hamandi K, Kleinschmidt A, Krakow K (2006) Linking generalized spike-and-wave discharges and resting state brain activity by using EEG/fMRI in a patient with absence seizures. *Epilepsia* 47(2):444–448.
42. Gotman J, et al. (2005) Generalized epileptic discharges show thalamocortical activation and suspension of the default state of the brain. *Proc Natl Acad Sci USA* 102(42):15236–15240.
43. Fransson P (2006) How default is the default mode of brain function? Further evidence from intrinsic BOLD signal fluctuations. *Neuropsychologia* 44(14):2836–2845.
44. Czisch M, et al. (2004) Functional MRI during sleep: BOLD signal decreases and their electrophysiological correlates. *Eur J Neurosci* 20(2):566–574.
45. Jahnke K, et al. (2012) To wake or not to wake? The two-sided nature of the human K-complex. *Neuroimage* 59(2):1631–1638.
46. Laufs H, et al. (2003) Electroencephalographic signatures of attentional and cognitive default modes in spontaneous brain activity fluctuations at rest. *Proc Natl Acad Sci USA* 100(19):11053–11058.
47. He BJ, Raichle ME (2009) The fMRI signal, slow cortical potential and consciousness. *Trends Cogn Sci* 13(7):302–309.
48. He BJ, Snyder AZ, Zempel JM, Smyth MD, Raichle ME (2008) Electrophysiological correlates of the brain's intrinsic large-scale functional architecture. *Proc Natl Acad Sci USA* 105(41):16039–16044.
49. Bak P, Tang C, Wiesenfeld K (1987) Self-organized criticality: An explanation of the 1/f noise. *Phys Rev Lett* 59(4):381–384.
50. Expert P, et al. (2011) Self-similar correlation function in brain resting-state functional magnetic resonance imaging. *J R Soc Interface* 8(57):472–479.
51. Tagliazucchi E, Balenzuela P, Fraiman D, Chialvo DR (2012) Criticality in large-scale brain FMRI dynamics unveiled by a novel point process analysis. *Front Physiol* 3:15.
52. Haimovici A, Tagliazucchi E, Balenzuela P, Chialvo DR (2013) Brain organization into resting state networks emerges at criticality on a model of the human connectome. *Phys Rev Lett* 110(17):178101.
53. Priesemann V, Valderrama M, Wibral M, Le Van Quyen M (2013) Neuronal avalanches differ from wakefulness to deep sleep—evidence from intracranial depth recordings in humans. *PLoS Comput Biol* 9(3):e1002985.
54. Allen PJ, Polizzi G, Krakow K, Fish DR, Lemieux L (1998) Identification of EEG events in the MR scanner: The problem of pulse artifact and a method for its subtraction. *Neuroimage* 8(3):229–239.
55. AASM (2007) *The AASM Manual for the Scoring of Sleep and Associated Events: Rules, Terminology and Technical Specifications* (American Academy of Sleep Medicine, Chicago).
56. Glover GH, Li TQ, Ress D (2000) Image-based method for retrospective correction of physiological motion effects in fMRI: RETROICOR. *Magn Reson Med* 44(1):162–167.
57. Lemieux L, Salek-Haddadi A, Lund TE, Laufs H, Carmichael D (2007) Modelling large motion events in fMRI studies of patients with epilepsy. *Magn Reson Imaging* 25(6):894–901.